Bottleneck effect in three-dimensional turbulence simulations

Wolfgang Dobler*

Kiepenheuer-Institut für Sonnenphysik, Schöneckstraße 6, D-79104 Freiburg, Germany

Nils Erland L. Haugen[†]

Department of Physics, The Norwegian University of Science and Technology, Høyskoleringen 5, N-7034 Trondheim, Norway

Tarek A. Yousef[‡]

Fluid Technology Group, Faculty of Engineering Science and Technology, NTNU, Kolbjørn Hejes vei 2B, N-7491 Trondheim, Norway

Axel Brandenburg[§]

NORDITA, Blegdamsvej 17, DK-2100 Copenhagen Ø, Denmark

At numerical resolutions around 512^3 and above, three-dimensional energy spectra from turbulence simulations begin to show noticeably shallower spectra than $k^{-5/3}$ near the dissipation wave number ("bottleneck effect"). This effect is shown to be significantly weaker in one-dimensional spectra such as those obtained in wind tunnel turbulence. The difference can be understood in terms of the transformation between the one-dimensional and three-dimensional energy spectra under the assumption that the turbulent velocity field is isotropic. Transversal and longitudinal energy spectra are similar and can both accurately be computed from the full three-dimensional spectra. Second-order structure functions are less susceptible to the bottleneck effect and may be better suited for inferring the scaling exponent from numerical simulation data.

PACS number(s): 47.27.Gs, 47.27.Ak, 47.11.+j, 47.27.Eq

I. INTRODUCTION

Based on dimensional analysis, Kolmogorov [1] concluded that the energy spectrum for isotropic hydrodynamic turbulence has the form

$$E(k) = C_K \epsilon^{2/3} k^{-5/3} \qquad (1)$$

for wave numbers k in the inertial range between the energy-carrying and the dissipation wave number $k_d = \epsilon^{1/4} \nu^{-3/4}$ (where ν denotes the kinematic viscosity, ϵ the spectral energy flux, and C_K is nowadays called the "Kolmogorov constant"). This scaling has been confirmed experimentally over several orders of magnitude [2,3]. Nevertheless, numerical simulations consistently show excess power just before the dissipation wave number k_d, which manifests itself particularly at high resolution [4]. This phenomenon has been named "bottleneck effect" [5,6] and is usually explained by the lack of smaller-scale vortices at wave numbers $k > k_d$, which makes the energy cascade less efficient around k_d. According to a related interpretation, the bottleneck effect is the consequence of viscosity stabilizing small vortex tubes against the kink instability [7].

The effect is particularly strong when an unphysical hyperviscosity is used; see Refs. [8,9] for results from two-dimensional hydromagnetic turbulence. In experimental data, on the other hand, the bottleneck effect is less pronounced

[10,11], and it has previously been noticed that it is much weaker when the one-dimensional energy spectra are used [9]. In the present paper we discuss a simple relation between the one-dimensional and three-dimensional energy spectra, which agrees well with the simulation data and explains this difference.

The data we use for discussing the bottleneck effect are from a weakly compressible isothermal three-dimensional forced turbulence simulation at a numerical resolution of 1024^3 grid points. The forcing has vanishing net helicity and the forcing wave number k_f is between 1 and 2. The box size is $L_x = L_y = L_z = 2\pi$, which discretizes the wave numbers in units of $k_1 = 1$. The viscosity ν is chosen such that the Reynolds number based on the inverse mean forcing wave number, $u_{\mathrm{rms}}/(\nu \bar{k}_f)$, is around 1700. The Taylor microscale is $\sqrt{5} u_{\mathrm{rms}}/\omega_{\mathrm{rms}} \approx 0.14$, where ω_{rms} is the root mean square vorticity, so the corresponding Taylor microscale Reynolds number is 350. The average dissipation rate ϵ is such that k_d/k_f is around 130. The root mean square Mach number is between 0.17 and 0.20; for this type of weakly compressible simulations, we find that the energies of solenoidal and potential components of the flow have a ratio $E_{\mathrm{pot}}/E_{\mathrm{sol}} \approx 10^{-4} - 10^{-2}$ for most scales; only towards the Nyquist frequency the ratio increases to about 0.1. Even for Mach numbers between 0.5 and 10, this ratio is only about 0.1–0.2 [12,13]. It is thus reasonable to assume that compressibility is irrelevant for the results presented here. This is also supported by the fact that incompressible pseudospectral simulations at a resolution of 1024^3 show a bottleneck effect [4].

The simulations discussed here were carried out using a high-order finite-difference code [14] and thus complement the results that have so far been obtained using spectral

───────────

*Electronic address: Wolfgang.Dobler@kis.uni-freiburg.de

[†]Electronic address: Nils.Haugen@phys.ntnu.no

[‡]Electronic address: Tarek.Yousef@mtf.ntnu.no

[§]Electronic address: Brandenb@nordita.dk

codes. Figure 1 shows the three-dimensional spectrum $E(k)$ together with the longitudinal and transversal one-dimensional spectra $E_L(k)$ and $E_T(k)$ in the upper panel. The "compensated spectra" in the lower panel allow easy identification of the bottleneck effect and show that it is practically present only in the three-dimensional spectrum $E(k)$.

In order to reduce the otherwise huge fluctuations, the one-dimensional spectra have been averaged horizontally,

$$E_L(k) = \frac{1}{N_x N_y} \sum_{p,q=1}^{N_x,N_y} |\tilde{u}_z(x_p, y_q, k)|^2, \qquad (2)$$

$$E_T(k) = \frac{1}{N_x N_y} \sum_{p,q=1}^{N_x,N_y} \tfrac{1}{2} |\tilde{u}_\perp(x_p, y_q, k)|^2, \qquad (3)$$

where $|\tilde{u}_\perp|^2 = |\tilde{u}_x|^2 + |\tilde{u}_y|^2$. Here

$$\tilde{\boldsymbol{u}}(x,y,k) = \left(\frac{L_z}{2\pi}\right)^{1/2} \frac{1}{N_z} \sum_{n=1}^{N_z} e^{ikz_n} \boldsymbol{u}(x,y,z_n) \qquad (4)$$

is the one-dimensional Fourier transform of the velocity vector $\boldsymbol{u}(\boldsymbol{x})$, and k scans the interval $[0, k_{\text{Ny}}] = [0, \pi/\delta z]$ at the resolution $\delta k = 2\pi/L_z$. The three-dimensional spectrum $E(k)$ has been obtained by integrating the three-dimensional spectral energy density over shells $k_i - \delta k/2 \leq k < k_i + \delta k/2$ in analogy to Eq. (A6), with $\delta k = 2\pi/L_x$ (and $L_x = L_y = L_z$). The spectra are normalized such that

$$\int_0^\infty E(k)\,dk = \frac{1}{2}\langle \boldsymbol{u}^2 \rangle = 3\int_0^\infty E_L(k)\,dk = 3\int_0^\infty E_T(k)\,dk. \qquad (5)$$

II. RELATIONS BETWEEN THE ONE- AND THREE-DIMENSIONAL SPECTRA

While most experimental measurements yield longitudinal one-dimensional spectra $E_L(k)$, the discussion of the relation between the one-dimensional (1D) and three-dimensional spectra is significantly simpler for the total one-dimensional spectrum $E_{1D}(k)$. We thus split this section in two parts: we first outline the relations for the total one-dimensional spectrum $E_{1D}(k)$, while in the second part we obtain analogous results for the longitudinal spectra, which are of direct relevance for experiments.

A. The total one-dimensional spectrum

The total one-dimensional spectrum $E_{1D}(k)$ is the sum of the longitudinal and twice (for the two directions) the transversal one-dimensional spectra,

$$E_{1D}(k) = E_L(k) + 2E_T(k). \qquad (6)$$

It is thus in some sense "more isotropic" than its constituents which results in simpler relations to the fully isotropic three-dimensional spectrum. In Sec. 1 of the Appendix we show that $E_{1D}(k)$ is related to $E(k)$ by
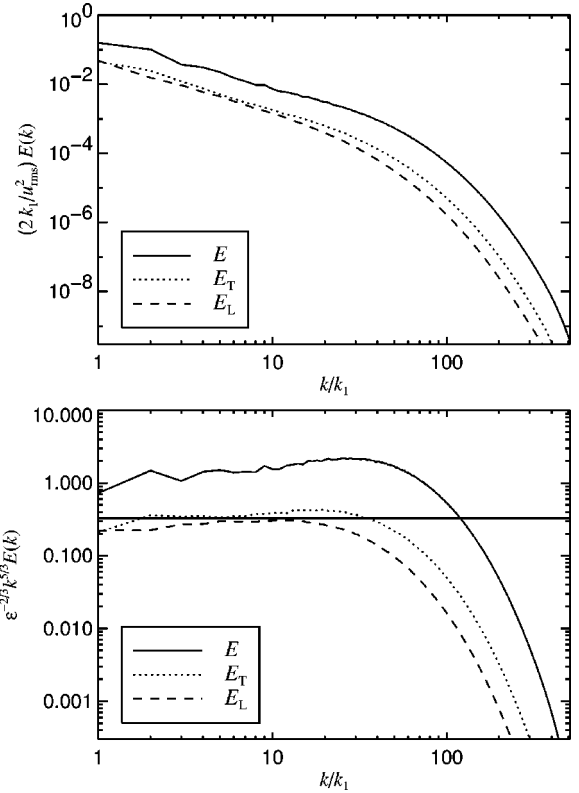

FIG. 1. Comparison of the averaged one-dimensional longitudinal and transversal spectra, $E_L(k)$ and $E_T(k)$, respectively, with the three-dimensional spectrum $E(k)$ for a forced turbulence simulation at 1024^3 grid points. Top: the spectra. Bottom: "compensated spectra" $\epsilon^{-2/3} k^{5/3} E(k)$, $\epsilon^{-2/3} k^{5/3} E_{L/T}(k)$; the horizontal line represents a $k^{-5/3}$ Kolmogorov spectrum. The local maximum of $E(k)$ around $k \approx 30$ represents the bottleneck effect. The dissipation wave number is $k_d = \epsilon^{1/4} \nu^{-3/4} \approx 200$.

$$E_{1D}(k) = \int_k^\infty \frac{E(k')}{k'} dk', \qquad (7)$$

which can also be inverted to give

$$E(k) = -k \frac{dE_{1D}}{dk}, \qquad (8)$$

provided the turbulence is isotropic. As $E(k)$ must be positive, Eq. (7) shows directly that the one-dimensional spectrum $E_{1D}(k)$ must be monotonously decreasing. On the other hand, no such restriction holds for $E(k)$, which is in fact increasing near $k=0$, since $E(0)=0$.

Equation (8) is a *local* relationship, and thus the functional form of $E(k)$ is fully determined by the local behavior of $E_{1D}(k)$ at a given wave number. To relate it to the bottleneck effect, we introduce the compensated spectra

$$\tilde{E}_{1D}(k) \equiv k^{5/3} E_{1D}(k), \quad \tilde{E}(k) \equiv k^{5/3} E(k), \qquad (9)$$

and rewrite Eq. (8) in the form

$$\widetilde{E}(k) = \left[\frac{5}{3} - \frac{d \ln \widetilde{E}_{1D}(k)}{d \ln k} \right] \widetilde{E}_{1D}(k). \qquad (10)$$

Several conclusions can be drawn from Eq. (10). First, if there is a finite interval where the Kolmogorov scaling (1) holds for the one-dimensional spectrum, then the same scaling will hold for the three-dimensional spectrum, and vice versa. Further, Eq. (10) shows explicitly that even if $\widetilde{E}_{1D}(k)$ is monotonous and nonincreasing, $\widetilde{E}(k)$ may show a maximum near k_d, provided that $\widetilde{E}_{1D}(k)$ bends towards the dissipative range sufficiently suddenly. For example, if the one-dimensional spectrum has the form

$$E_{1D}(k) = k^{-5/3} \exp[-(k/k_d)^n], \qquad (11)$$

then for small wave numbers k the compensated three-dimensional spectrum behaves like

$$\widetilde{E}(k) \approx \frac{5}{3} + \left(n - \frac{5}{3} \right) \left(\frac{k}{k_d} \right)^n \quad (\text{for } k \ll k_d), \qquad (12)$$

which shows that there will be a bottleneck effect in the three-dimensional spectrum when the one-dimensional spectrum falls off with an exponent $n > 5/3$. Finally, if $E_{1D}(k)$ shows a bottleneck effect, i.e., $\widetilde{E}_{1D}(k)$ shows a local maximum at some wave number k_m, then Eq. (10) shows that $\widetilde{E}(k)$ will also have an enhanced value there, $\widetilde{E}(k_m) = (5/3)\widetilde{E}_{1D}(k_m)$, and thus the three-dimensional spectrum $E(k)$ must show a bottleneck effect, too.

B. The longitudinal and transversal one-dimensional spectra

For isotropic turbulence, the one-dimensional longitudinal and transversal spectra are related to the three-dimensional spectrum by (see Sec. 2 of the Appendix)

$$E_L(k) = \frac{1}{2} \int_k^\infty \left(1 - \frac{k^2}{k'^2} \right) \frac{E(k')}{k'} dk', \qquad (13)$$

$$E_T(k) = \frac{1}{4} \int_k^\infty \left(1 + \frac{k^2}{k'^2} \right) \frac{E(k')}{k'} dk', \qquad (14)$$

and

$$E(k) = k^2 E_L''(k) - k E_L'(k) \qquad (15)$$

(the primes denoting derivatives). Differentiating Eq. (13), we obtain

$$E_L'(k) = -k \int_k^\infty \frac{E(k')}{k'^3} dk' < 0, \qquad (16)$$

which shows that $E_L(k)$ [just like $E_{1D}(k)$] must be monotonously decreasing.

Equation (15) is again a local relationship, and thus the functional form of $E(k)$ is fully determined by the local behavior of $E_L(k)$ at a given wave number. As in Eq. (9), we introduce the compensated spectra

$$\widetilde{E}(k) \equiv k^{5/3} E(k), \quad \widetilde{E}_L(k) \equiv k^{5/3} E_L(k), \qquad (17)$$

and rewrite Eq. (15) in the form

$$\widetilde{E} = \frac{55}{9} \widetilde{E}_L - \frac{13}{3} k \widetilde{E}_L' + k^2 \widetilde{E}_L''. \qquad (18)$$

The conclusions that can be drawn from Eq. (18) are similar to those for $E_{1D}(k)$. If there is a finite interval where the Kolmogorov scaling $E_L(k) = C_K^L \epsilon^{2/3} k^{-5/3}$ holds for the longitudinal spectrum (which implies $\widetilde{E}_L' = \widetilde{E}_L'' = 0$), then the same scaling will hold for the three-dimensional spectrum, and vice versa. The Kolmogorov constant C_K of the three-dimensional spectrum is then a factor $55/9 \approx 6.1$ larger than the corresponding constant C_K^L for $E_L(k)$; cf. Eq. (16.37 ′) of Ref. [15].

Equation (18) shows that even if $\widetilde{E}_L(k)$ is monotonously nonincreasing, $\widetilde{E}(k)$ may show a maximum near k_d, provided that the term involving $\widetilde{E}_L'$ dominates over the curvature term $k^2 \widetilde{E}_L''$. Finally, if $E_L(k)$ shows a bottleneck effect, then beyond the local maximum, $\widetilde{E}_L'(k) < 0$. If the maximum is wide enough, Eq. (18) implies that $\widetilde{E}$ will show a bottleneck effect, too. The situation is less clear if $k_m^2 \widetilde{E}_L''(k_m)$ is large [corresponding to a narrow maximum of $\widetilde{E}_L(k)$], but numerical experiments with model spectra suggest that the three-dimensional spectrum $\widetilde{E}_L(k)$ will still be nonmonotonous, although it may vary in a more complicated manner.

III. SAMPLE SPECTRA

A. Model spectra

For illustration purposes, we consider a longitudinal spectrum of the form

$$E_L(k) = \left(\frac{k}{k_d} \right)^{-5/3} \exp[-(k/k_d)^n]. \qquad (19)$$

The compensated spectrum $\widetilde{E}_L(k) \equiv (k/k_d)^{5/3} E_L(k) = \exp[-(k/k_d)^n]$ is monotonously decreasing and thus $E_L(k)$ shows no bottleneck effect at all. At $k = k_d$ the compensated three-dimensional spectrum has the value

$$\widetilde{E}(k_d) = e^{-1} \left(\frac{55}{9} + \frac{16}{3} n \right), \qquad (20)$$

which shows that $\widetilde{E}(k_d) > 55/9$ (a sufficient condition for the bottleneck effect in the three-dimensional spectrum) if $n > (55/48)(e-1) \approx 1.97$; this is illustrated in Fig. 2. A more thorough analysis reveals that $\widetilde{E}(k)$ will have a maximum if and only if $n > 5/3$, but for $n \lesssim 2$ the maximum is hardly discernible.

As we have seen, in order to get a bottleneck effect, we need a one-dimensional spectrum with a more complicated form than just $k^{-5/3} \exp(-k/k_d)$. One functional form where this is given has been proposed by She and Jackson [10], based on experimental data:
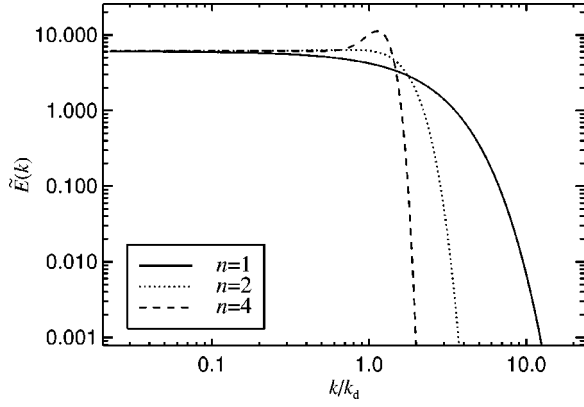
FIG. 2. Compensated three-dimensional spectrum $\widetilde{E}(k)$ $=(k/k_d)^{5/3}E(k)$ corresponding to the longitudinal spectrum (19) for exponents $n=1,2,4$. The bottleneck effect appears for $n\gtrsim 2$.

$$\frac{E_L(k)}{E_L(k_p)}=\left[\left(\frac{k}{k_p}\right)^{-5/3}+0.8\left(\frac{k}{k_p}\right)^{-1}\right]e^{-0.63k/k_p}. \quad (21)$$

Figure 3(a) shows this spectrum [for $E_L(k_p)=k_p=1$], together with the corresponding three-dimensional spectrum (15). The compensated spectra clearly show a bottleneck effect in the three-dimensional spectrum, which is (practically) absent in the one-dimensional spectrum.

Quian [16] has proposed a spectrum that shows quite a marked bottleneck effect. Based on a closure model, he suggests the functional form

$$E(k)=\epsilon^{2/3}k^{-5/3}\left[1.19+6.31\left(\frac{k}{k_d}\right)^{2/3}\right]\exp[-5.4(k/k_d)^{4/3}]. \quad (22)$$

Figure 3(b) shows the longitudinal and three-dimensional spectra. For this model, the bottleneck effect is very prominent in $E(k)$, and also evident (although weaker) in the longitudinal one-dimensional spectrum $E_L(k)$.

B. Spectra from direct numerical simulations

1. Three-dimensional spectrum from $E_L(k)$

To avoid (double) numerical differentiation of our spectra, we use a parametrization for $E_L(k)$. The one-dimensional spectrum shown in Fig. 1 is well approximated by the formula

$$E_L^{(p)}(k)=(\hat{k}^{-5/3}+a_0\hat{k}^{a_1})e^{-a_2\hat{k}}\frac{a_3+a_4\hat{k}+a_5\hat{k}^2}{1+a_6\hat{k}+a_7\hat{k}^2}, \quad (23)$$

with

$$a_i=(2.1\times10^{-8},4.3,0.42,0.85,1.2,0.00048,-0.0068,0.34),$$

where $\hat{k}\equiv k/k_p$. The peak dissipation wave number $k_p\approx 18$ is the location of the maximum of the dissipation spectrum k^2E_L, and is about one order of magnitude smaller than k_d [10]. Figure 4 shows the parametrized one-dimensional spec-
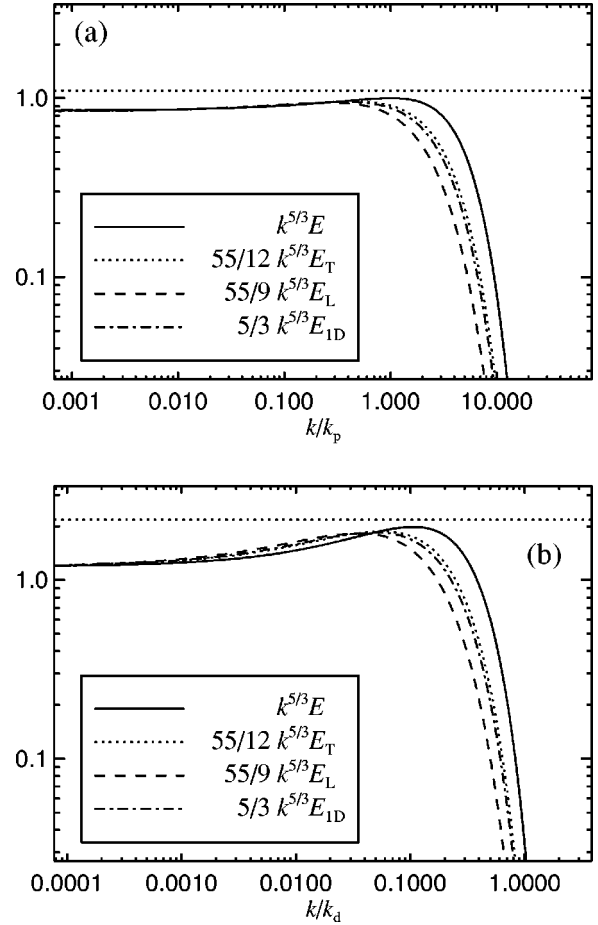

FIG. 3. Comparison of compensated spectra $\widetilde{E}_L(k)$ and $\widetilde{E}(k)$ for the models of She and Jackson, and of Quian. (a) Longitudinal spectrum (21), together with the derived three-dimensional spectra, longitudinal and total 1D spectra; the spectra are normalized according to $k_p=E_L(k_p)=1$. Note the appearance of a mild bottleneck effect, i.e., a maximum in $\widetilde{E}(k)$. (b) Three-dimensional spectrum (22), together with the derived one-dimensional spectra; the spectra are normalized according to $k_d=\epsilon=1$. The bottleneck effect is quite pronounced and appears in both, one- and three-dimensional spectra. Note that in both plots, the amplitudes of the one-dimensional spectra have been scaled to get matching plateaus in the inertial range. The dotted horizontal lines are drawn for orientation.

trum $E_L(k)$ according to Eq. (23), together with the derived three-dimensional spectrum $E(k)$ from Eq. (15). Also shown are data points from the numerical simulation (diamonds and crosses). Comparing the calculated three-dimensional profile (solid line) with the data points (crosses), we find that Eq. (15) agrees quite well with the numerical data for not too small k. The discrepancy for very small wave numbers can be explained by the fact that the periodicity of the numerical box precludes isotropy at the largest scales.

It is quite evident from Fig. 4 that $\widetilde{E}(k)$ shows a much more pronounced local maximum near the dissipation wave number k_d than does $\widetilde{E}_L(k)$. The width and structure of the maximum is well reproduced by Eq. (15) applied to our parametrization (23) of $E_L(k)$.
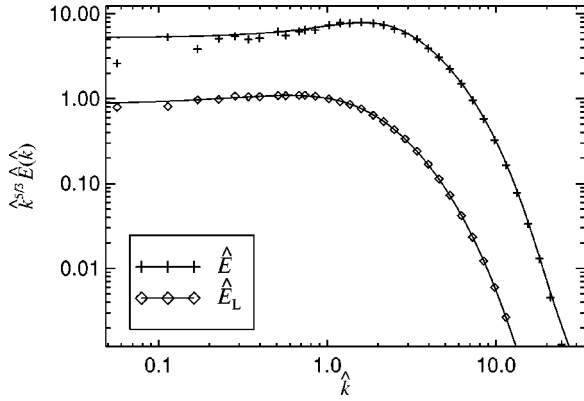
FIG. 4. Compensated longitudinal energy spectrum $\hat{k}^{5/3}\hat{E}_L(\hat{k})$ according to parametrization (23) and the corresponding three-dimensional spectrum $\hat{k}^{5/3}\hat{E}(\hat{k})$ from Eq. (15). For comparison, crosses and diamonds show the spectra obtained directly from the simulation. The spectra have been normalized by introducing $\hat{k} \equiv k/k_p$, $\hat{E}_L \equiv E_L/E_L(k_p)$, and $\hat{E} \equiv E/E_L(k_p)$, where k_p is the peak dissipation wave number. The three-dimensional energy spectrum agrees quite well with the numerical data for $k \geq 4\,\delta k$, where $\delta k = 2\pi/L_x \approx 0.06 k_p$ is the wave number resolution.

2. One-dimensional spectra from $E(k)$

In contrast to experiments, data from numerical simulations easily provide the three-dimensional spectrum $E(k)$. Sometimes it may be interesting to determine the one-dimensional spectra $E_L(k)$ and $E_T(k)$ from the three-dimensional spectrum. The corresponding relations (13) and (14) were given above. Here we apply them to our numerical data to see how well the inferred one-dimensional spectra agree with those directly obtained from the simulation data. Figure 5 shows the longitudinal and transversal spectra obtained by applying Eqs. (13) and (14) to the three-dimensional spectrum using the trapezoidal rule. The agree-
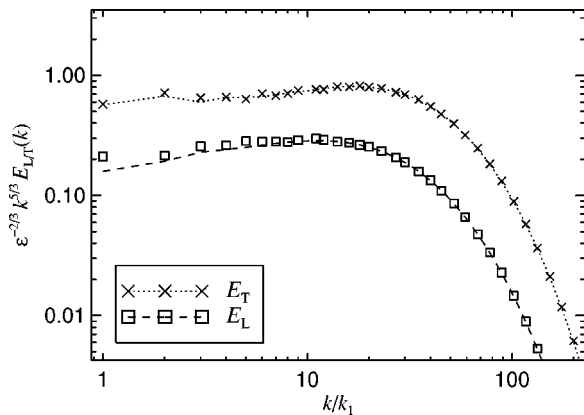

FIG. 5. Compensated one-dimensional energy spectra. Shown are the longitudinal spectrum $E_L(k)$ and the transversal spectrum $E_T(k)$. Data points obtained directly from the numerical simulation are indicated as boxes (E_L) and crosses (E_T). The dashed and dotted lines show the one-dimensional spectra obtained from Eqs. (13) and (14), respectively. The spectra agree quite well with the numerical data for $k \geq 2\,\delta k$.

ment is quite good for both one-dimensional spectra apart from the very lowest wave number.

IV. STRUCTURE FUNCTIONS

Another classical tool in turbulence research is the investigation of structure functions [6]. The second-order structure function

$$S_2(r) = \langle [u(x) - u(x+r)]^2 \rangle \qquad (24)$$

is related to the three- and one-dimensional spectra via the Fourier-type integral transforms (cf. Ref. [15])

$$S_2(r) = 4 \int_0^\infty \left(1 - \frac{\sin kr}{kr} \right) E(k)\,dk \qquad (25)$$

$$= 4 \int_0^\infty (3 - 3\cos kr + kr\sin kr) E_L(k)\,dk. \qquad (26)$$

Similarly, the longitudinal and transversal second-order structure functions

$$S_2^{(L)}(r) = \langle [u_z(x) - u_z(x+r\hat{z})]^2 \rangle, \qquad (27)$$

$$S_2^{(T)}(r) = \langle [u_z(x) - u_z(x+r\hat{x})]^2 \rangle \qquad (28)$$

can be expressed as

$$S_2^{(L/T)}(r) = 4 \int_0^\infty (1 - \cos kr) E_{L/T}(k)\,dk. \qquad (29)$$

Localized variations of $E(k)$ or $E_L(k)$ in wave number space, such as the bottleneck effect, will influence $S_2(r)$ and $S_2^{(L/T)}(r)$ in a nonlocal fashion. Correspondingly, little insight into the bottleneck effect can be expected from structure functions. On the other hand, this means that structure functions are less sensitive to the bottleneck effect and might thus form a more robust tool for assessing scaling exponents and possibly even the Kolmogorov constant at moderate Reynolds number.

However, while structure functions are much smoother than spectra, their scaling range is considerably smaller, which adds its own difficulties to that method. In three numerical simulations at 256^3, 512^3, and 1024^3 grid points, we find the value of the structure function exponent derived from $S_2(r)$ to be 0.74, 0.67, and 0.68, respectively, which is quite close to Kolmogorov's value of 2/3. However, if we use the two transversal and the longitudinal structure functions (corresponding to the z displacement of the u_x, u_y, and u_z components of the velocity vector), the values are far less accurate and span the intervals [0.67,0.79], [0.62,0.72], [0.60,0.72], respectively, for the three resolutions, which indicates that the convergence may not have yet been reached.

The situation for the Kolmogorov constant is even worse, because from $S_2(r)$ we get the values 3.96, 1.93, 1.8, respectively, for the three resolutions. So in practice, the slow convergence may well render this method more unreliable than the use of one-dimensional spectra.
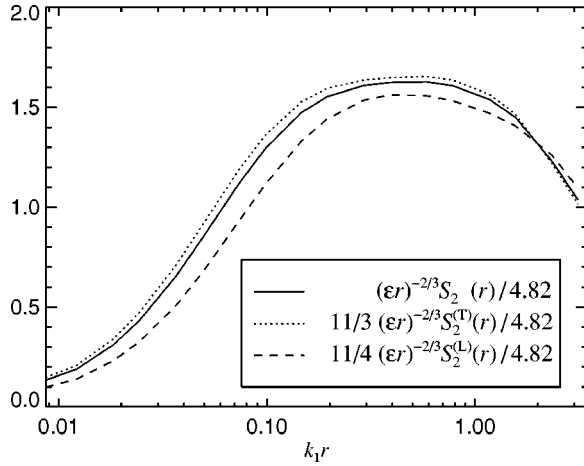
FIG. 6. Compensated second-order structure functions from our direct numerical simulation data. The amplitudes have been scaled to get matching plateaus representing the Kolmogorov constant C_K.

Similar to the spectra, the second-order structure functions can be transformed into each other (assuming isotropy) according to the relations

$$S_2(r) = r \frac{dS_2^{(L)}(r)}{dr} + 3S_2^{(L)}(r), \tag{30}$$

$$S_2^{(L)}(r) = \frac{1}{r^3} \int_0^r S_2(r') r'^2 dr', \tag{31}$$

$$S_2^{(T)}(r) = \frac{S_2(r) - S_2^{(L)}(r)}{2}. \tag{32}$$

Like in the case of relations (13)–(15), this has implications for the monotonicity of the compensated structure functions $\tilde{S}(r) \equiv Sr^{-2/3}(r)$ near the boundaries of the scaling interval; see also Ref. [6]. Normally, however, none of the structure functions $S_2(r)$, $S_2^{(L)}(r)$, $S_2^{(T)}(r)$ show a secondary bump near the edges of the scaling interval, as can be seen in Fig. 6, which implies that we cannot directly apply the results of Secs. II and III to structure functions.

V. CONCLUSIONS

In this paper, we have highlighted the discrepancy between the one-dimensional and three-dimensional spectra. Well-known relations between the spectra show that the three-dimensional spectrum may show the bottleneck effect even if the one-dimensional spectra do not show it at all, while the converse cannot happen. The spectra always agree in the inertial range, $E(k) \propto E_L(k) \propto k^{-5/3}$, but in current numerical simulations the length of the inertial range is limited to about one decade, so the discrepancy is quite noticeable. Indeed, the topic of a bottleneck effect in hydrodynamic turbulence has only emerged in the past ten years since numerical simulations have shown this to be a strong effect. On the other hand, the relation linking one-dimensional to three-

dimensional spectra has been known for 50 years, but it has to our knowledge never been explicitly discussed in connection with the bottleneck effect. In the present paper, we have shown that much of the bottleneck effect seen in numerical turbulence simulations is simply the result of the mathematical discrepancy between the one- and three-dimensional spectra.

The bottleneck effect has no evident manifestation in the second-order structure functions, where localized features in k space appear in a delocalized manner. This implies that in order to obtain the asymptotic energy spectrum exponent it may be easier to use second-order structure function exponents, although in practice the reduced scaling range may render this method difficult.

APPENDIX: RELATIONS BETWEEN THE ONE- AND THREE-DIMENSIONAL SPECTRA

In this appendix, we derive the relations between the three-dimensional spectrum $E(k)$ and the one-dimensional spectra $E_L(k)$, $E_L(k)$, $E_{1D}(k)$, most of which can also be found in Refs. [15,17,18].

1. Total one-dimensional spectrum

We derive the relation between the three-dimensional spectrum $E(k)$ and the total one-dimensional spectrum $E_{1D}(k) \equiv E_L(k) + 2E_T(k)$. Consider a periodic box of volume $V = L_x L_y L_z$ with a turbulent velocity field $\boldsymbol{u}(\boldsymbol{x})$, which has the Fourier transform

$$\hat{\boldsymbol{u}}(\boldsymbol{k}) = \frac{1}{\sqrt{(2\pi)^3 V}} \int_V e^{i\boldsymbol{k}\cdot\boldsymbol{x}} \boldsymbol{u}(\boldsymbol{x}) dx^3, \tag{A1}$$

with the inversion

$$\boldsymbol{u}(\boldsymbol{x}) = \sqrt{\frac{V}{(2\pi)^3}} \int e^{-i\boldsymbol{k}\cdot\boldsymbol{x}} \hat{\boldsymbol{u}}(\boldsymbol{k}) dk^3. \tag{A2}$$

The one-dimensional kinetic energy spectrum is

$$E_{1D}(k_z) = 2 \int \int \frac{\langle |\hat{\boldsymbol{u}}(\boldsymbol{k})|^2 \rangle}{2} dk_x dk_y \quad (k_z \geq 0), \tag{A3}$$

where $\langle \cdot \rangle$ denotes an ensemble average and $\boldsymbol{k} = (k_x, k_y, k_z)$. The factor 2 in Eq. (A3) accounts for the fact that E_{1D} does not distinguish between positive and negative k_z. Normalization of $E_{1D}(k_z)$ is such that

$$\int_0^\infty E_{1D}(k_z) dk_z = \frac{u_{\mathrm{rms}}^2}{2} \equiv \frac{1}{V} \int_V \frac{\langle |\boldsymbol{u}(\boldsymbol{x})|^2 \rangle}{2} dx^3. \tag{A4}$$

Equation (A3) can also be written as the xy average

$$E_{1D}(k_z) = \frac{1}{L_x L_y} \int \langle |\tilde{u}(x,y,k_z)|^2 \rangle dx dy \qquad (A5)$$

and is for homogeneous turbulence equal to $\langle |\tilde{u}(x,y,k_z)|^2 \rangle$ at any point (x,y).

The three-dimensional velocity energy spectrum is given by

$$E(k) \equiv \int_{4\pi} \frac{\langle |\hat{u}(k)|^2 \rangle}{2} k^2 d\Omega_k, \qquad (A6)$$

where $d\Omega_k$ denotes the solid angle element in k space. $E(k)$ satisfies the relation

$$\int_0^\infty E(k) dk = \frac{u_{rms}^2}{2}. \qquad (A7)$$

If u is statistically isotropic in the sense that the ensemble average of the spectral energy of the velocity $\langle |u(k)|^2 \rangle$ is only a function of $k = |k|$, then $E(k)$ becomes

$$E(k) = 4\pi k^2 \frac{\langle |\hat{u}(k)|^2 \rangle}{2}. \qquad (A8)$$

To evaluate E_{1D} in this case, we introduce cylindrical coordinates (κ, ϕ, k_z) in k space and write the double integral (A3) in the form

$$E_{1D}(k_z) = 2 \int_0^\infty \frac{\langle |\hat{u}(k)|^2 \rangle}{2} 2\pi \kappa d\kappa = 4\pi \int_{k_z}^\infty \frac{\langle |\hat{u}(k)|^2 \rangle}{2} k dk, \qquad (A9)$$

since $\kappa^2 = k^2 - k_z^2$. Comparing with Eq. (A8), we see that

$$E_{1D}(k_z) = \int_{k_z}^\infty \frac{E(k)}{k} dk, \qquad (A10)$$

the inversion of which gives

$$E(k) = -k \frac{dE_{1D}(k)}{dk} = -E_{1D} \frac{d\ln E_{1D}(k)}{d\ln k}. \qquad (A11)$$

2. The longitudinal and transversal one-dimensional spectra

In this section, we derive the relation between the longitudinal and transversal one-dimensional energy spectra $E_L(k)$, $E_T(k)$, and the three-dimensional energy spectrum $E(k)$.

For homogeneous, isotropic turbulence, the energy spectrum tensor is given by (see, e.g., Refs. [15,17,18])

$$F_{pq}(k) \equiv \langle \hat{u}_p(k) \hat{u}_q^*(k) \rangle = [F_L(k) - F_T(k)] \frac{k_p k_q}{k^2} + F_T(k) \delta_{pq}. \qquad (A12)$$

If we assume incompressibility, the longitudinal component F_L vanishes, and thus

$$F_{pq}(k) = \left(\delta_{pq} - \frac{k_p k_q}{k^2} \right) F_T(k) = \left(\delta_{pq} - \frac{k_p k_q}{k^2} \right) \frac{E(k)}{4\pi k^2}, \qquad (A13)$$

and in particular

$$2\pi F_{zz}(k) = \left(1 - \frac{k_z^2}{k^2} \right) \frac{E(k)}{2k^2}, \qquad (A14)$$

$$2\pi [F_{xx}(k) + F_{yy}(k)] = \left(1 + \frac{k_z^2}{k^2} \right) \frac{E(k)}{2k^2}. \qquad (A15)$$

The longitudinal one-dimensional spectrum

$$E_L(k_z) \equiv 2 \int \int \frac{F_{zz}(k)}{2} dk_x dk_y \qquad (A16)$$

thus becomes

$$E_L(k_z) = \int_0^\infty F_{zz}(k) 2\pi \kappa d\kappa = \frac{1}{2} \int_{k_z}^\infty \left(1 - \frac{k_z^2}{k^2} \right) \frac{E(k)}{k} dk, \qquad (A17)$$

using the same substitution as in Eq. (A9) above. Similarly, we can write the transversal one-dimensional spectrum

$$E_T(k_z) \equiv 2 \int \int \frac{F_{xx}(k) + F_{yy}(k)}{4} dk_x dk_y, \qquad (A18)$$

in the form

$$E_T(k_z) = \frac{1}{4} \int_{k_z}^\infty \left(1 + \frac{k_z^2}{k^2} \right) \frac{E(k)}{k} dk. \qquad (A19)$$

Taking the derivative of Eq. (A17), we find

$$\frac{E_L'(k_z)}{k_z} = - \int_{k_z}^\infty \frac{E(k)}{k^3} dk, \qquad (A20)$$

and thus

$$E(k) = k^2 E_L''(k) - k E_L'(k). \qquad (A21)$$

Inserting this relation into Eq. (A19) allows us to express $E_T(k)$ through $E_L(k)$ as

$$E_T(k) = -k \frac{E_L'(k)}{2} + \frac{E_L(k)}{2}. \qquad (A22)$$

[1] A.N. Kolmogorov, C. R. Acad. Sci. URSS **30**, 301 (1941).

[2] F.H. Champagne, J. Fluid Mech. **86**, 67 (1978).

[3] K.R. Sreenivasan, Phys. Fluids **7**, 2778 (1995).

[4] T. Gotoh and D. Fukayama, Phys. Rev. Lett. **86**, 3775 (2001); T. Gotoh, Comput. Phys. Commun. **147**, 530 (2002).

[5] G. Falkovich, Phys. Fluids **6**, 1411 (1994).

[6] D. Lohse and A. Müller-Groeling, Phys. Rev. Lett. **74**, 1747 (1995); Phys. Rev. E **54**, 395 (1996).

[7] P.R. Woodward, D.H. Porter, B.K. Edgar, S.E. Anderson, and G. Basset, Comput. Appl. Math. **14**, 97 (1995).

[8] D. Biskamp, E. Schwarz, and A. Celani, Phys. Rev. Lett. **81**, 4855 (1998).

[9] D. Biskamp and W.-C. Müller, Phys. Plasmas **7**, 4889 (2000).

[10] Z.-S. She and E. Jackson, Phys. Fluids A **5**, 1526 (1993); see also S. Panchev and D. Kesich, C. R. Acad. Bulg. Sci. **22**, 627 (1969).

[11] S.G. Saddoughi and S.V. Veeravalli, J. Fluid Mech. **268**, 333 (1994).

[12] D.H. Porter, P.R. Woodward, and A. Pouquet, Phys. Fluids **10**, 237 (1998).

[13] S. Boldyrev, Å. Nordlund, and P. Padoan, Astrophys. J. **573**, 678 (2002).

[14] We use the Pencil Code which is a cache-efficient high-order finite-difference code (sixth order in space and third order in time) for solving the compressible hydrodynamic and magnetohydrodynamics equations; http://www.nordita.dk/data/brandenb/pencil-code

[15] A.S. Monin and A.M. Yaglom, *Statistical Fluid Mechanics* (MIT Press, Cambridge, MA, 1987), Vol. 2, Sec. 12.

[16] J. Quian, Phys. Fluids **27**, 2229 (1984).

[17] G.K. Batchelor, *The Theory of Homogeneous Turbulence* (Cambridge University Press, Cambridge, 1953), p. 50.

[18] J.O. Hinze, *Turbulence*, 2nd ed. (McGraw-Hill, New York, 1975), p. 202.